NATIONAL AERONAUTICS AND SPACE ADMINISTRATION

Technical Report No. 32-793

Development of a Point Damper for the Ranger Solar Panels

M. Gayman

JET PROPULSION LABORATORY
CALIFORNIA INSTITUTE OF TECHNOLOGY
PASADENA, CALIFORNIA

September 1, 1965

NATIONAL AERONAUTICS AND SPACE ADMINISTRATION

Technical Report No. 32-793

Development of a Point Damper for the Ranger Solar Panels

M. Gayman

M. G. Comuntzis

M. G. Comuntzis, *Manager*
Lunar Spacecraft Development Section

JET PROPULSION LABORATORY
CALIFORNIA INSTITUTE OF TECHNOLOGY
PASADENA, CALIFORNIA

September 1, 1965

Prepared Under Contract No. NAS 7-100
National Aeronautics & Space Administration

CONTENTS

TABLES

FIGURES

FIGURES (Cont'd)

ABSTRACT

10419

The increase in solar panel size on *Rangers 6* through 9 over those used on prior *Ranger* flights resulted in intolerably higher structural gains during simulated-launch vibration testing. Rather than adding more solar panel attachments as a remedy, dampers were designed to absorb some of the input energy from the spacecraft. Of the three types of dampers considered, the one selected, on the basis of probable availability within schedule, demonstrated satisfactory reduction of the dynamic gains.

The damper design, geometry, and discussion of the assembly and test equipment are included in this Report. Data reduction is given in detail, and damper development results are discussed.

I. INTRODUCTION

The flight-launch configuration of solar panels for *Rangers 6* through 9 consisted of each panel supported from the spacecraft structure at two hinge points and at two latch points (Fig. 1).[1] With the increased solar panel size on the Block III configuration (*Rangers 6* through 9), the initial spacecraft-assembly Type-Approval-Level shake tests indicated panel-tip structural gains of 50 times the input at the spacecraft base (corresponding to stresses in excess of material yield) with the panels supported with "rigid links" at the latch points.

Two possible solutions were evident at the time: (1) the addition of a third latch point to the solar panel tip, as shown in Fig. 2, or (2) replacement of the two rigid links with dampers which would absorb some of the input energy from the spacecraft structure. Provided that a satisfactory damper could be developed within the available schedule time, solution 2 was considered preferable because it required a less complex system and no additional interface to the TV instrument.

At this point in the schedule, the design requirements for the damper were:

1. To use the two existing latch points on the structure.
2. To use the existing solar-panel structure hinge points and latch points.
3. To stay within the allowable shroud envelope for all possible excursions during launch.
4. To reduce the panel tip gains to an acceptable structural level of about 20 (i.e., the ratio of tip acceleration to the input acceleration at the spacecraft base).
5. To deliver tested prototype damper units in 8 wk for a complete spacecraft Structural-Test-Model test (to verify the developed design requirements at the unit level).

[1]The panels used on prior *Ranger* flights were smaller but were satisfactorily supported in a similar manner with "rigid links."

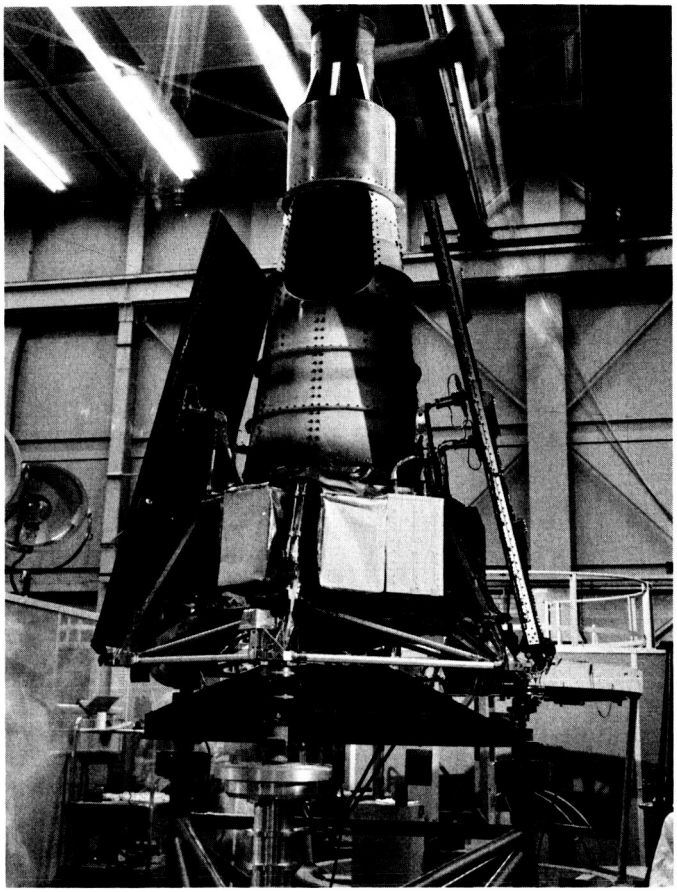

Fig. 1. *Ranger*-spacecraft flight configuration

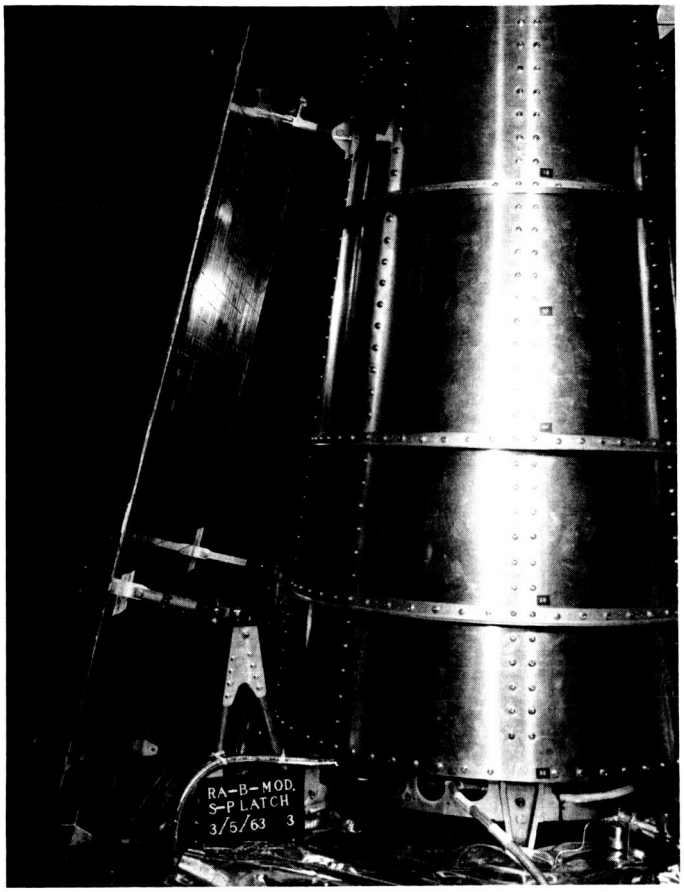

Fig. 2. Three rigid solar-panel latch links

II. DESIGN APPROACH

The combined requirements that the damper serve as a locating link for the solar panel and that it be deflected in order to absorb energy dictated a parallel spring/damper configuration. Furthermore, the damper must be located at a point on the panel that did not include any of the lower bending or combined bending and torsion nodes. In order to satisfy these requirements, an approximate check of the probable lower order nodal points was made to see if the design requirement of preselected latch points was at all acceptable. This check indicated that latch points were removed sufficiently from the important nodes.

The selection of the spring constant was a compromise between a desired minimum value for maximum damper effectiveness and a desired maximum for panel location and damper centering. Fortunately, the limited allowable

damper deflection, which was imposed by the schedule-dictated design requirements, was geometrically compatible with the available envelope for the solar-panel deflection. The spring constant was then selected on the basis of the panel static launch accelerations plus the anticipated dynamic excursions.

The selection of the damping coefficient was not so straightforward. A design employing a nearly linear damping coefficient was selected as a target, since this would permit the easiest data reduction for unit tests and would simplify any structural analysis that might be made. Because of the structural complexity of the total spacecraft, no parametric structural analysis had been made to determine the optimum damping coefficient for the dampers. Existing circumstances, primarily schedule, forced the philosophy of selecting a damping coefficient to critically damp the panel ($C/C_0 > 1.0$) in its rigid-body mode for the minimum operation coefficient (Fig. 3). Then tests at the subassembly and complete assembly level were made to see whether the dampers would reduce the panel-tip gains to the acceptable level. To gain some early confidence in range of damping and spring constant, a single panel similar to the flight configuration was shaken on a rigid fixture using some nonflight-type design dampers (Fig. 4). As demonstrated in Fig. 5, the results were encouraging; at least a single panel is relatively insensitive to the change in damping in the range of $1.1 \leq C/C_0 \leq 4.5$.

Three types of dampers were considered; all expected to be nearly linear with velocity:

1. The first damper was to be a piston inside of a larger diameter "rigid" cylinder that contained a low-viscosity fluid and the spring. One end of the piston rod and the opposite end of the cylinder would form the attachments to the spacecraft and solar panel. As the piston was forced through the cylinder, the fluid on one end would be forced through the annular space to the opposite end; provided the Reynolds number were low enough, the force would be proportional to the piston velocity. This is referred to as the "*Ranger* damper" in the following parts of this Report.

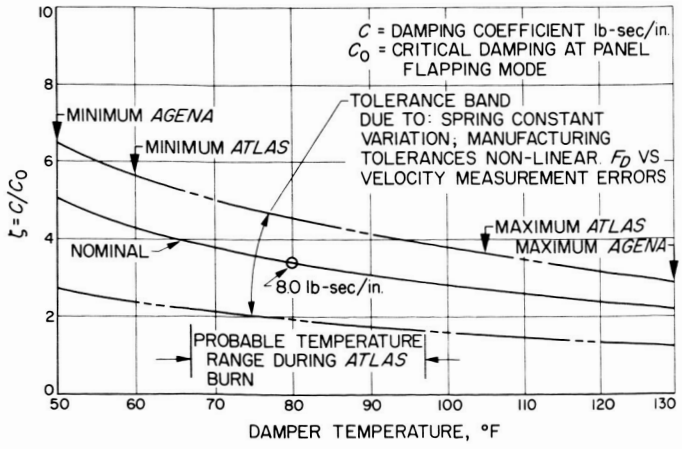

Fig. 3. Basis for selecting design damping coefficient

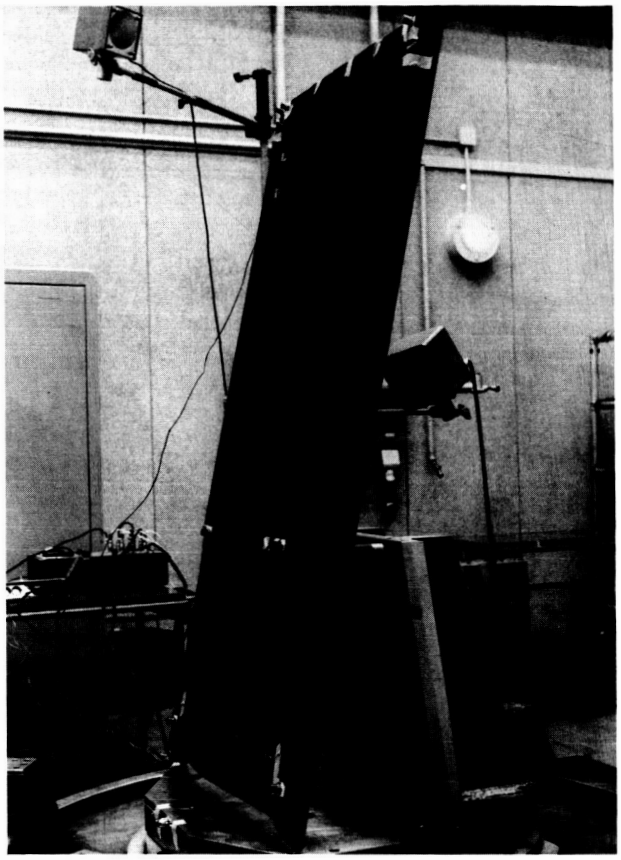

Fig. 4. Preliminary damper feasibility test using solar panel

2. The second damper considered was similar to the first except that the outer case containing the fluid would be a Bellows that could be a completely welded-up assembly, thus avoiding dynamic seals that could leak. The Bellows spring constant would serve as part or all of the required spring. This is referred to as the "Bellows damper" in the subsequent parts of this Report.

3. The third possible damper was composed of two concentric tubes with the small annular gap filled with a high-viscosity fluid. Opposite ends of the two tubes would form the attachments to the spring and to the spacecraft and solar panel.

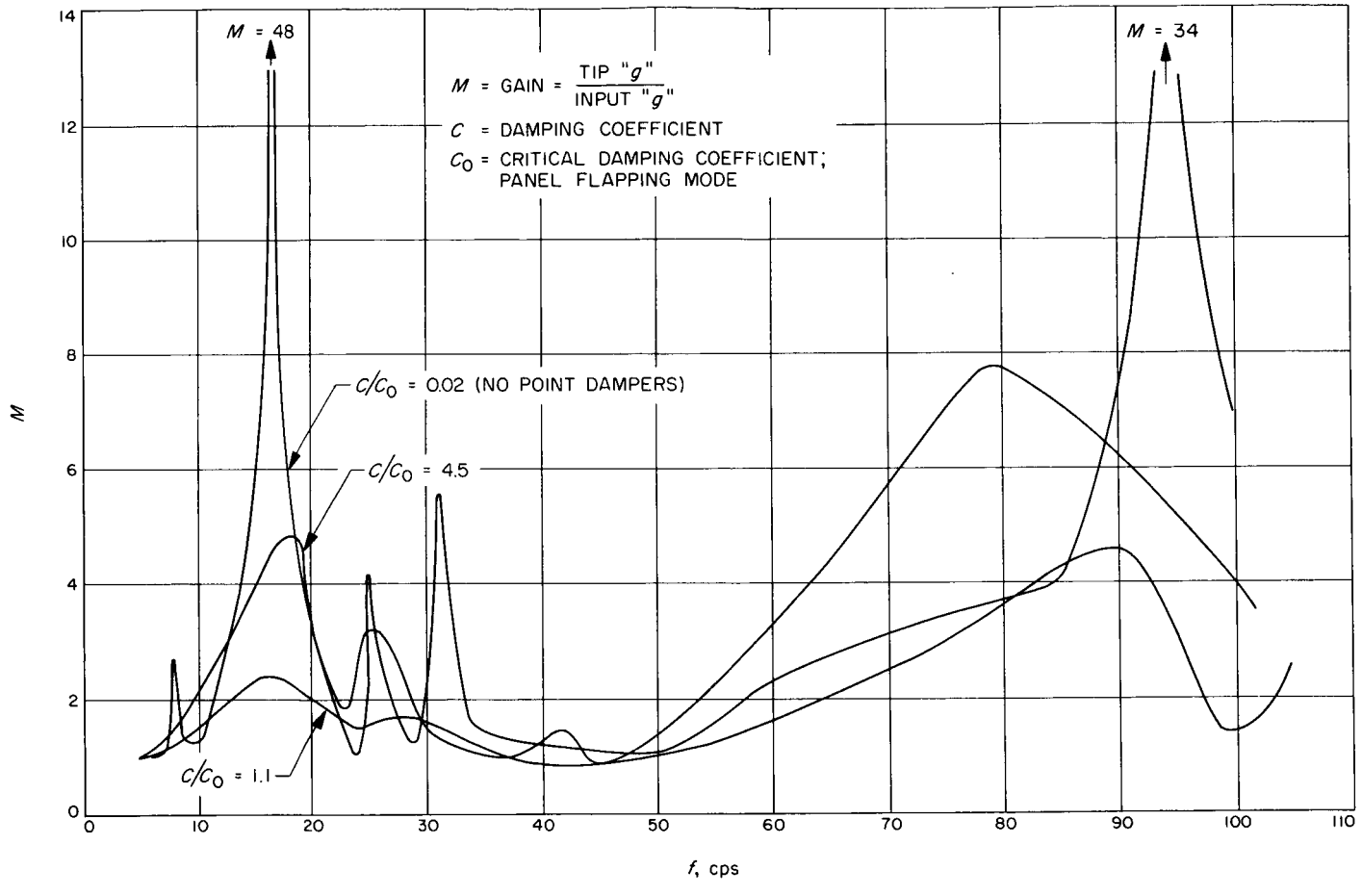

Fig. 5. Preliminary tests of feasible damping-coefficient range

Subsequent tests showed that only the first of these three types of dampers closely approached linear damping.

Although the third type is the simplest conceptually, early tests on some prototype units gave little confidence in the possibility of reliably establishing and maintaining, with use, a completely filled annular space. Test results on nominally identical hardware gave widely varying damping coefficients, which also changed with testing cycles; this approach was dropped as a feasible concept. (It should be noted that some of these problems have been solved, since this type of damper has been used on a later spacecraft program.)

The design, in flight configuration, was completed for both of the first two types of dampers listed. The performance of these dampers is given in the remainder of this Report. Prior to any fabrication the first was selected as the probable flight unit solely on the basis that it was the only hope of getting a satisfactory damper within the available schedule time.

The *Ranger* damper is shown in Fig. 6; Fig. 7 shows the Bellows damper. The *Ranger* damper and its solar-panel pyrotechnic-release latch is shown in Fig. 8. The manner of latching the solar panel to the spacecraft during the launch phase (Fig. 1) is shown in more detail in Fig. 9.

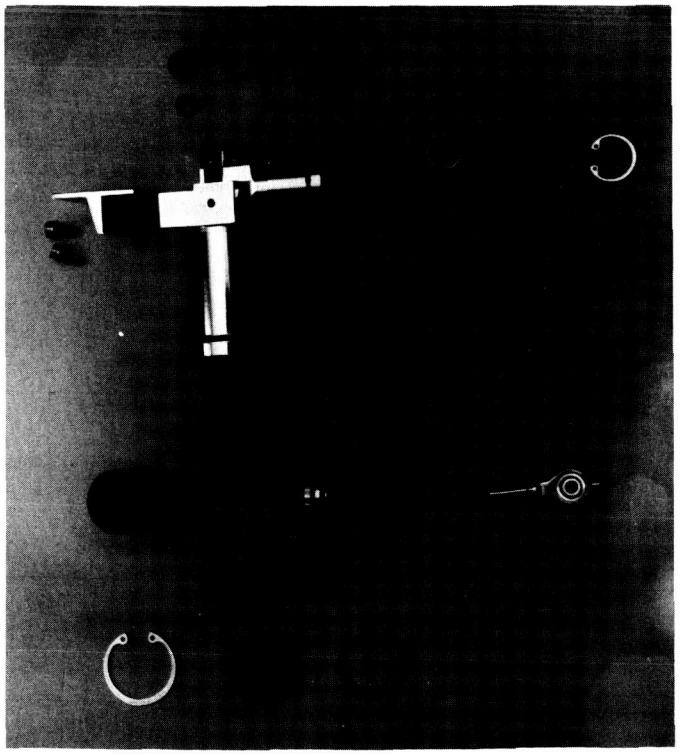

Fig. 6. *Ranger* damper

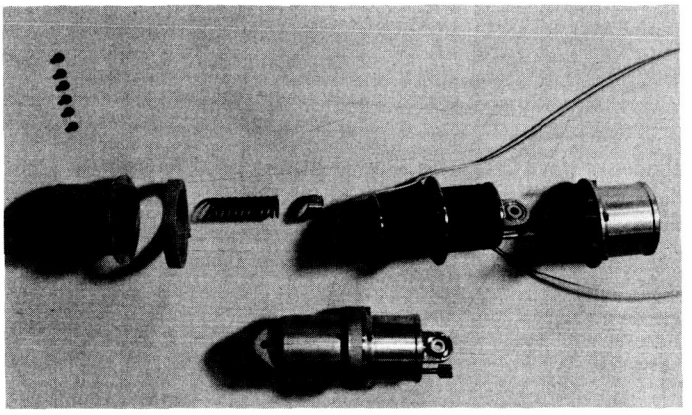

Fig. 7. Bellows damper

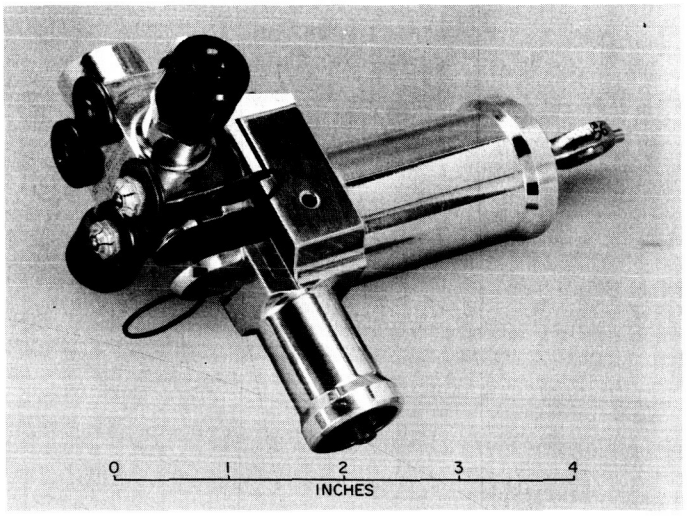

Fig. 8. *Ranger* damper assembled with pyrotechnic latch

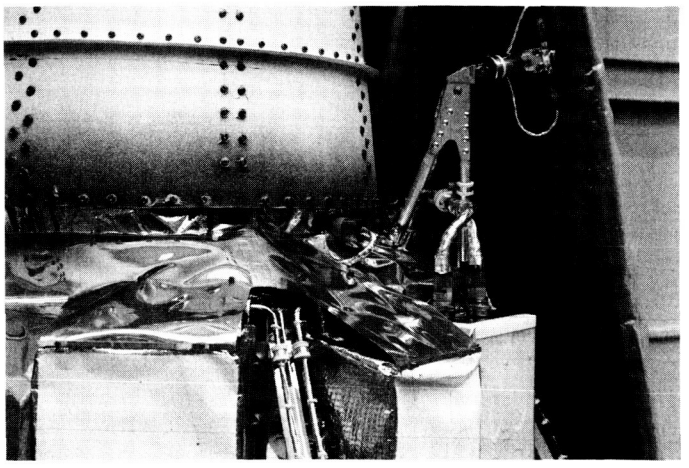

Fig. 9. *Ranger* damper assembled to spacecraft

III. DETAIL DESIGN

The damper geometry was based on the relationships developed below, using Figs. 10 and 11 and the listed nomenclature:

p = fluid pressure in annular space, lb/in.^{2}

$P = (p_1 - p_2)$ = pressure difference across piston, lb/in.^{2}

V = piston velocity relative to cylinder, in./sec

u = fluid velocity in annular space, in./sec

v = average fluid velocity in annular space, in./sec

q = fluid flow rate through annular space, in.^{3}/sec in. = in.^{2}/sec

μ = fluid viscosity, lb-sec/in.^{2}

The general Navier Stokes equation for viscous fluid flow is valid and reduces to:

$$-\frac{\partial p}{\partial x_f} + u\frac{\partial^2 u}{\partial y^2} = 0$$

assuming a long annular space, $L >> h$; continuous flow, $\partial u/\partial t = 0$; no circumferential or radial flow; incompressible fluid; and inertia forces $<<$ viscous forces. Also

$$\frac{\partial p}{\partial x_f} = -\frac{P}{L}$$

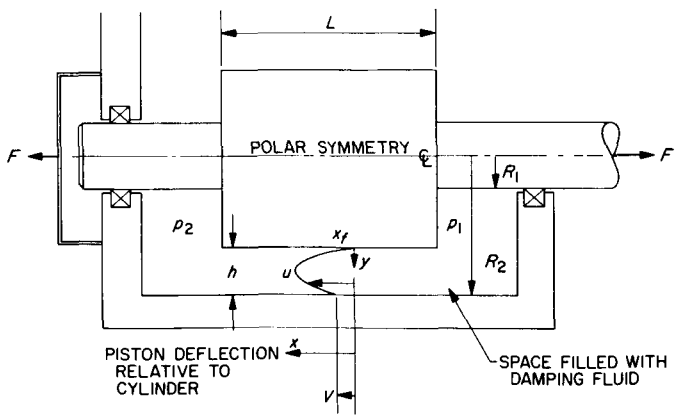

Fig. 10. Schematic model of *Ranger* damper

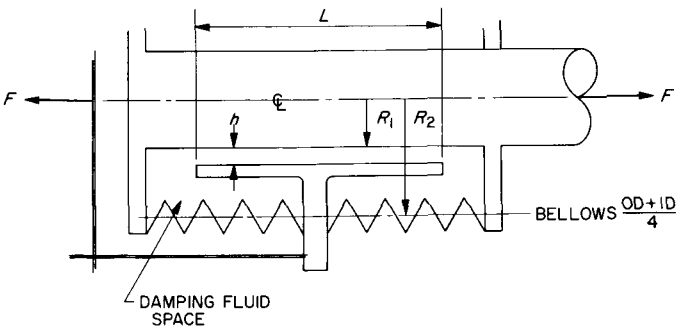

Fig. 11. Schematic model of Bellows damper

so

$$\frac{d^2u}{dy^2} = -\frac{P}{\mu L} = A_1 \qquad (1)$$

$$\frac{du}{dy} = A_1 y + A_2$$

$$u = \frac{A_1 y^2}{2} + A_2 y + A_3$$

Substituting boundary conditions at $u = 0$,

$$y = 0 \rightarrow A_3 = 0$$

at $y = h$,

$$u = V \rightarrow A_2 = \frac{V}{h} - \frac{A_1 h}{2}$$

$$u = A_1 y^2 + y\left(\frac{V}{h} - \frac{A_1 h}{2}\right)$$

The flow is

$$q = \int_0^h u\,dy = \int_0^h \left[\frac{A_1 y^2}{2} + \left(\frac{V}{h} - \frac{A_1 h}{2}\right) y\right] dy$$

$$q = \frac{A_1 h}{6} + \left(\frac{V}{h} - \frac{A_1 h}{2}\right)\frac{h^2}{2}$$

the average velocity, $v = q/h$

$$v = \frac{A_1 h}{6} + \left(\frac{V}{h} - \frac{A_1 h}{2}\right)\frac{h}{2} = -\frac{A_1 h^2}{12} + \frac{V}{2}$$

Substituting the value of A_1 from Eq. (1)

$$v = \frac{Ph^2}{12\mu L} + \frac{V}{2} \tag{2}$$

For continuity

v (area of annular space) = V (area of cylinder − area of rod)

$$v = \frac{V}{2h} \frac{(R_2^2 - R_1^2)}{\left(R_2 - \frac{h}{2}\right)} \tag{3}$$

The force/pressure relationship is

$$F = P\pi \left[\left(R_2 - \frac{h}{2} \right)^2 - R_1^2 \right] \tag{4}$$

Combining Eqs. (2), (3), and (4) yields:

$$V = \frac{Fh^3}{6\pi\mu LB} \tag{5}$$

where

$$B = \left[\left(R_2 - \frac{h}{2} \right)^2 - R_1^2 \right] \left[\frac{(R_2^2 - R_1^2)}{\left(R_2 - \frac{h}{2} \right)} - h \right]$$

At any particular time

$$V = \dot{x}$$

and

$$F = C\dot{x},$$

so

$$C = \frac{6\pi\mu LB}{h^3}, \tag{6}$$

where C is the damping coefficient, lb-sec/in.; and $\dot{x}$ is the piston velocity with respect to the cylinder, in./sec.

IV. ASSEMBLY AND TEST EQUIPMENT

For consistent performance of a damper and for consistency between damper units, the fluid cavity must be filled, with no voids. The apparatus developed to fulfill this requirement is shown in Fig. 12. The procedure is to hold the apparatus and empty dampers at 10^{-3} to 10^{-4} mm hg for 4 hr to assure removal of essentially all of the gas from the damper, then to introduce the fluid that is de-aerated by allowing it to flow slowly from the reservoir over the bubble tower. The spring-constant checking is done on the fixture, shown in Fig. 13. These and other detailed assembly and performance check procedures are outlined in JPL Specification RCP-31529-DTL.

The damper performance (i.e., determination of the damping coefficient C) is done by driving one end of the damper in sinusoidal motion with the other end connected to ground, at various frequencies and displacements. The value of C is then determined from the component of the driving force in phase with the velocity.

During the first part of the damper-development program, a hydraulic shaker (Fig. 14) and an electromechanical shaker (Fig. 15), were used to generate this motion. The use of this equipment for this purpose proved to have several drawbacks:

1. Output did not faithfully represent $x = A \sin \omega t$ at all of the frequencies and displacements of interest.
2. Tests consumed excessive technician man-hours per data point.

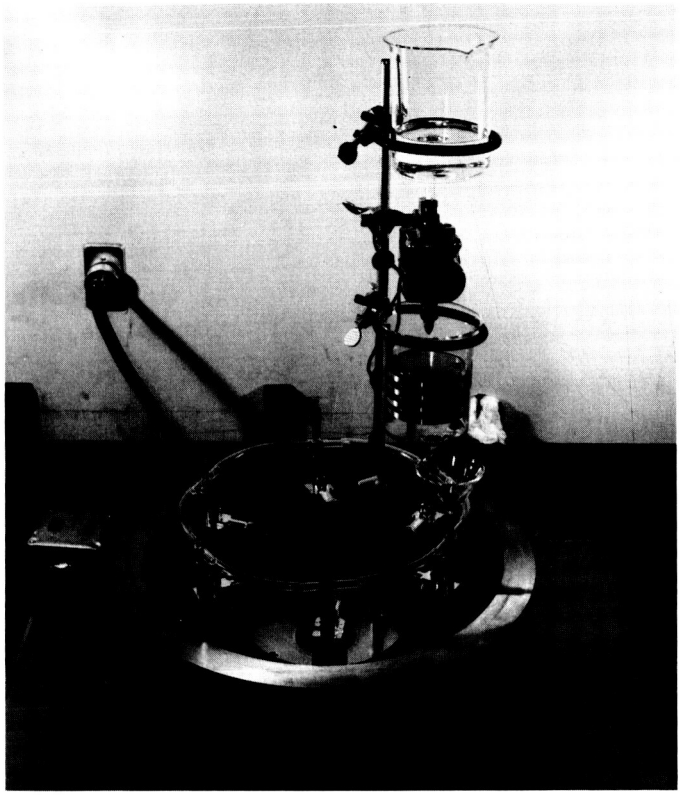

Fig. 12. Damper vacuum-filling apparatus

3. Machine utilization for other Laboratory tests was high, causing delays.

4. Instrumentation available for data recording made data reduction costly in man-hours.

In order to overcome these drawbacks, a "scotch yoke" sinusoidal displacement generator was designed and built to test the dampers. The machine (referred to as the "Inca Test Rig") and instrumentation rack are shown in Figs. 16, 17, and 18. It was conservatively designed to drive against a 200-lb load at the following frequencies and amplitudes:

A, in.	Cycles/sec
0.025	3 to 70
0.050	3 to 70
0.100	3 to 40
0.250	3 to 15

For all practical purposes, the machine velocity vs time output is unaffected by load; typical direct-recorded-performance curves are shown in Fig. 19.

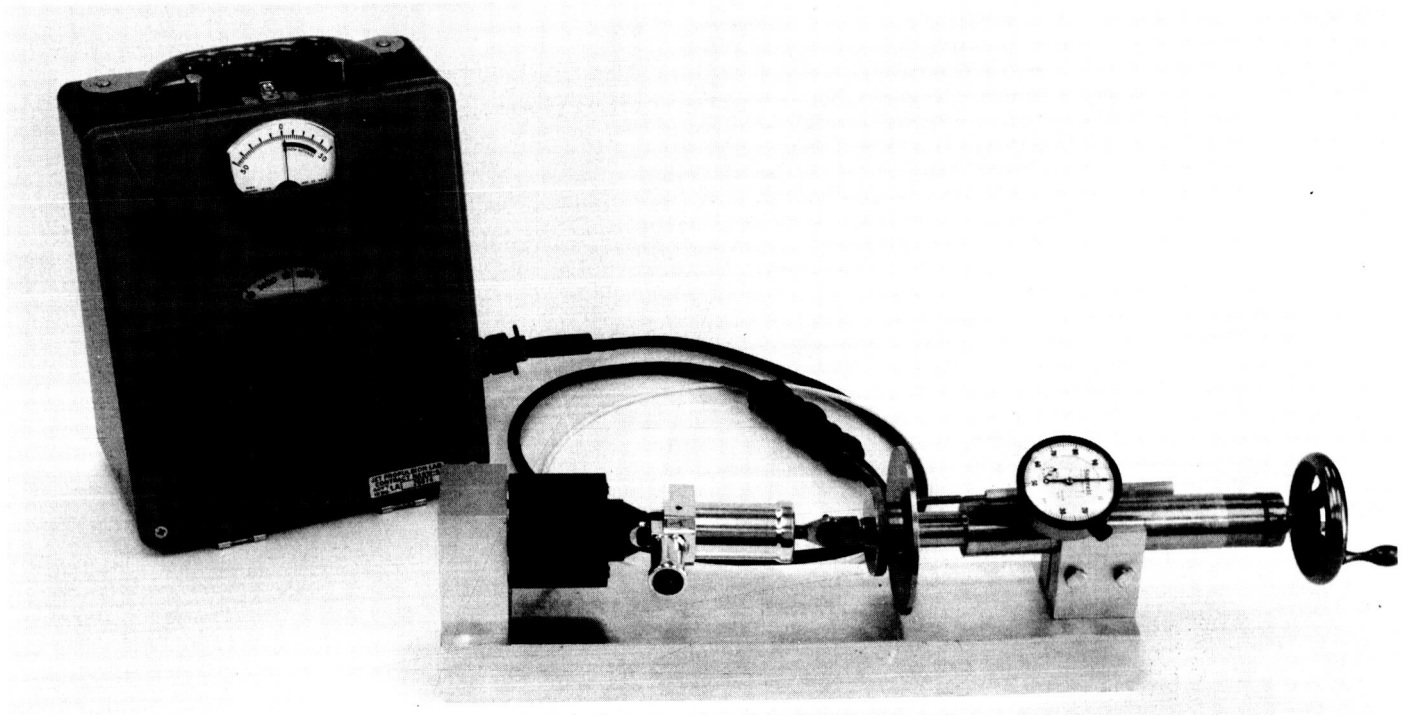

Fig. 13. Damper spring-check equipment

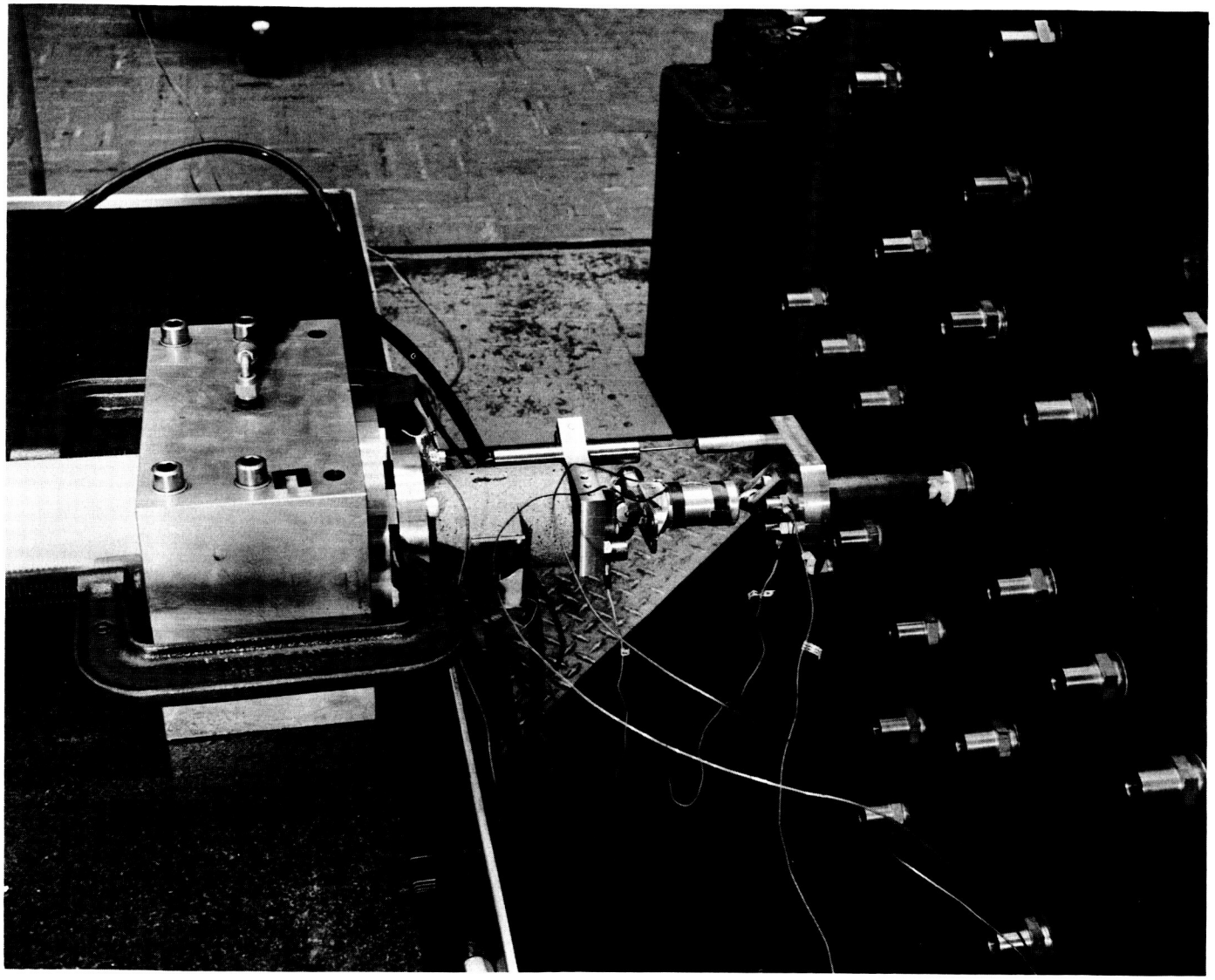

Fig. 14. *Ranger* damper mounted on hydraulic shaker for coefficient tests

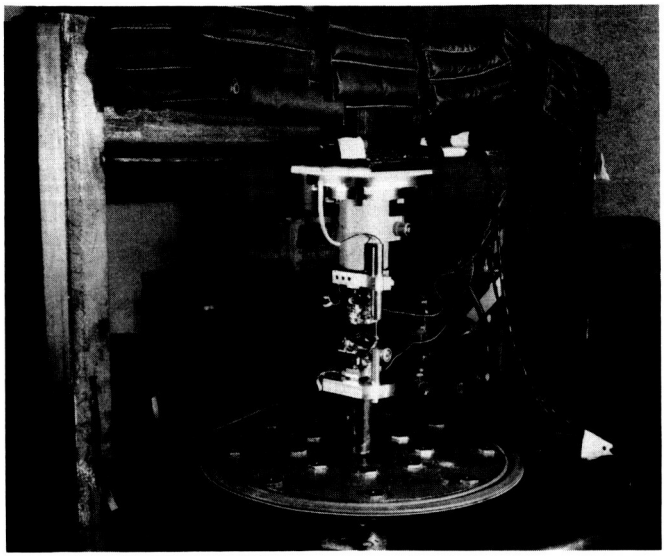

Fig. 15. *Ranger* damper (thermally insulated) mounted on electromechanic shaker for coefficient tests

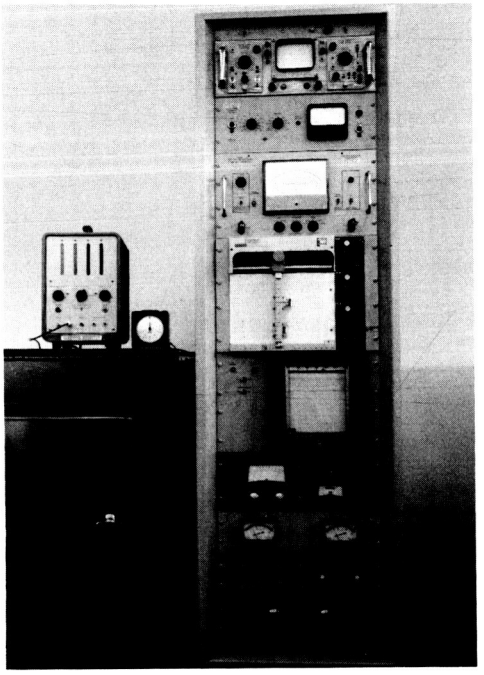

Fig. 17. Instrumentation rack for Inca test machine

Fig. 16. Inca damper-test machine

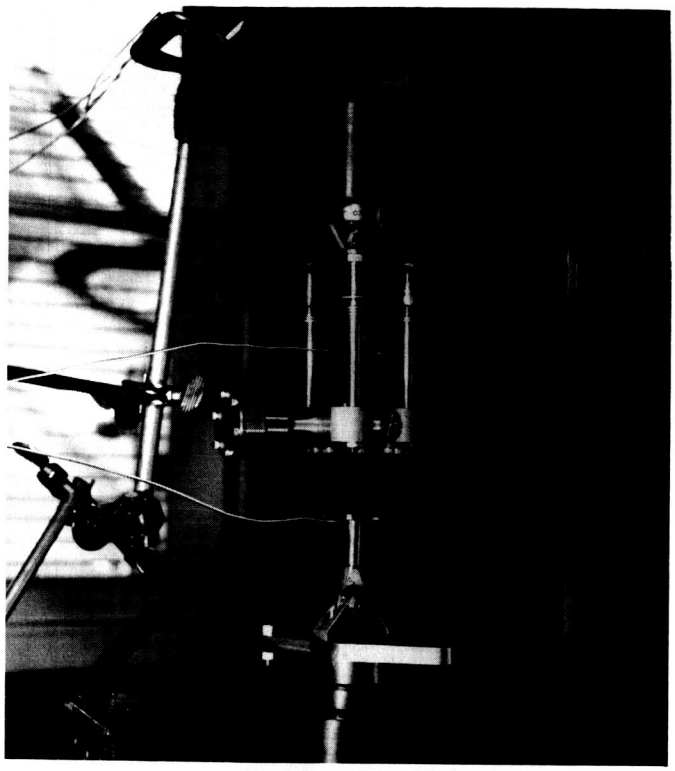

Fig. 18. Prototype Bellows damper mounted for testing on Inca machine

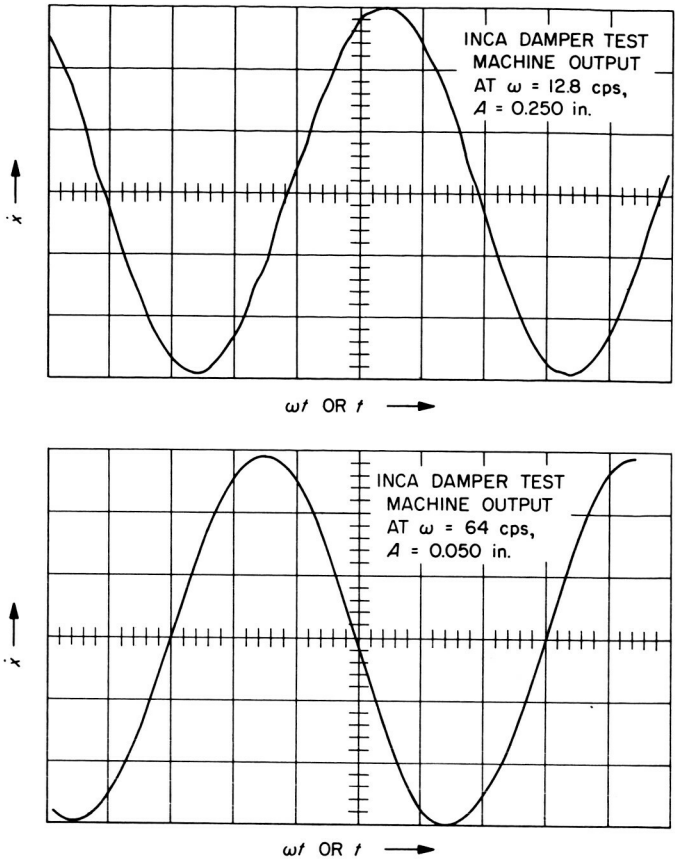

Fig. 19. Velocity output of Inca damper-test machine

V. TEST RESULTS AND DATA REDUCTION

All the test data on the individual units were reduced on the basis of the following assumptions, which are considered reasonably precise for the geometry of these dampers:

$$F = C\dot{x} + kx$$

$$x = A \sin \omega t$$

$$k = a_0 + a_1 (C\,|\dot{x}|) + a_2 (C\,|\dot{x}|)^2$$

$$F_{measured} = F_{max}$$

In the case of the *Ranger* dampers, $a_1 = 0$ and $a_2 = 0$ so it can be shown that:

$$C = \frac{1}{\omega A} (F_{max}^2 - k^2 A^2)^{1/2}$$

In the case of the Bellows damper, the spring constant varies with the change in internal pressure that forces the fluid through the annular space; thus, the data reduction

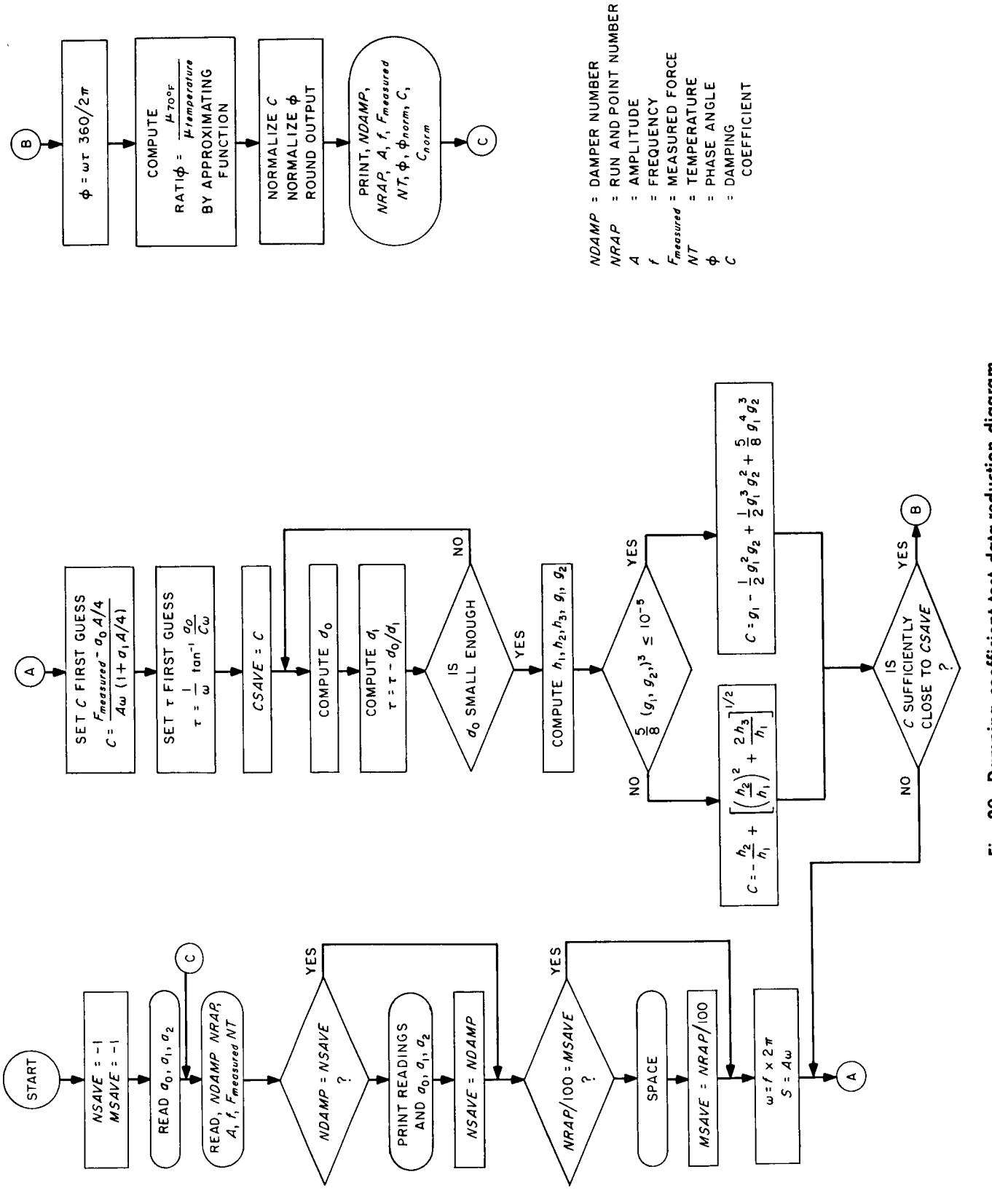

Fig. 20. Damping-coefficient test-data reduction diagram

is more involved. The iterative method[2] is given at the end of this section and diagramed in Fig. 20. The variation of k with internal pressure is shown in Fig. 21.

Finally, all reduced data were normalized to the same temperature to allow a common basis for comparison. The curve of μ vs temperature for the damping fluid used is given in Fig. 22.

Figure 23 illustrates a typical curve for the damping force measured on prototype *Ranger* dampers; Fig. 24 gives the measured damping coefficients of all of the flight-damper units. Part or all of this data, except for the last four units shown on Fig. 24, was obtained using the shakers. The last four units were tested solely on the Inca Test Rig and show considerably less data scatter, thus

[2]Developed by R. Chamberlain for this data reduction process.

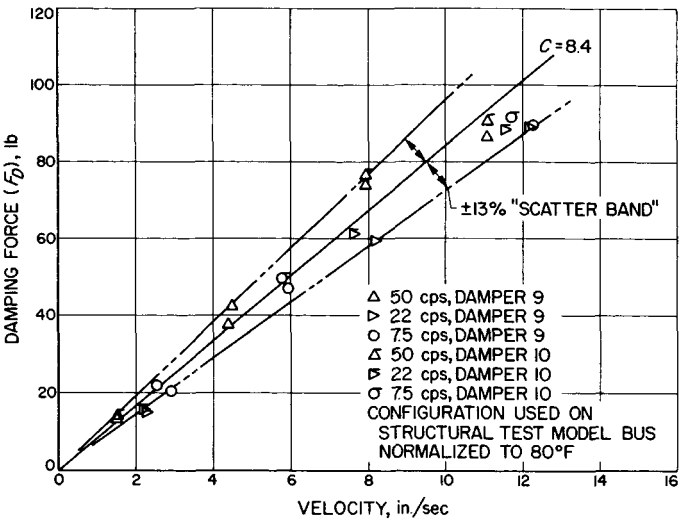

Fig. 23. Typical performance of *Ranger* dampers

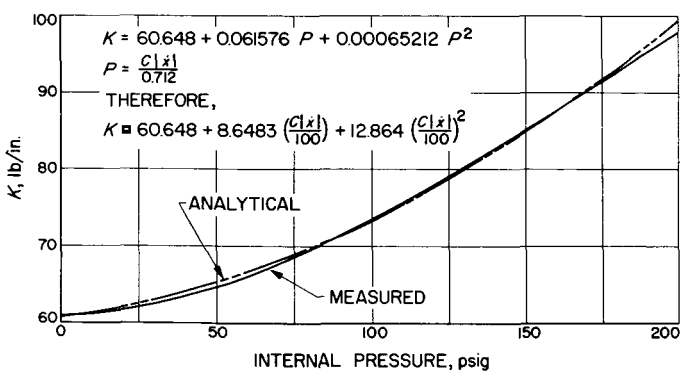

Fig. 21. Bellows damper: variation of spring constant with pressure

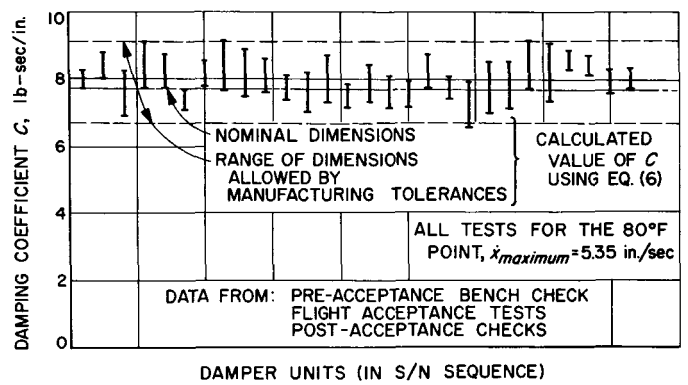

Fig. 24. Performance of *Ranger* flight-unit dampers

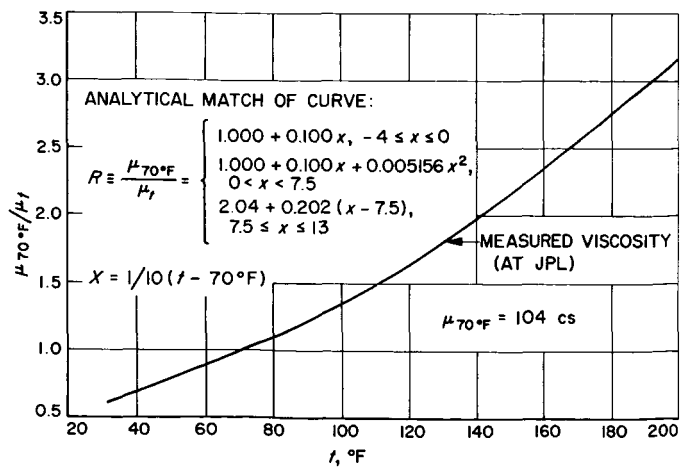

Fig. 22. Damping fluid variation of viscosity with temperature

giving a more realistic picture of the actual damper performance.

In the assumptions made for data reduction, the fluid-acceleration term was neglected because its effect was calculated to be within the magnitude of experimental error. For tests run at different amplitudes for the same value of $\dot{x}_{max}$, this term, $\ddot{x}_{max} \approx 1/A$ so the driving force necessary to accelerate the fluid decreases with increasing amplitude. This effect is just perceptible in Fig. 23.

The curves (Figs. 25 through 29) and summary (Fig. 30) show the performance of the bellows dampers. The damping performance is much less predictable by analysis than that of the *Ranger* damper and they demonstrate

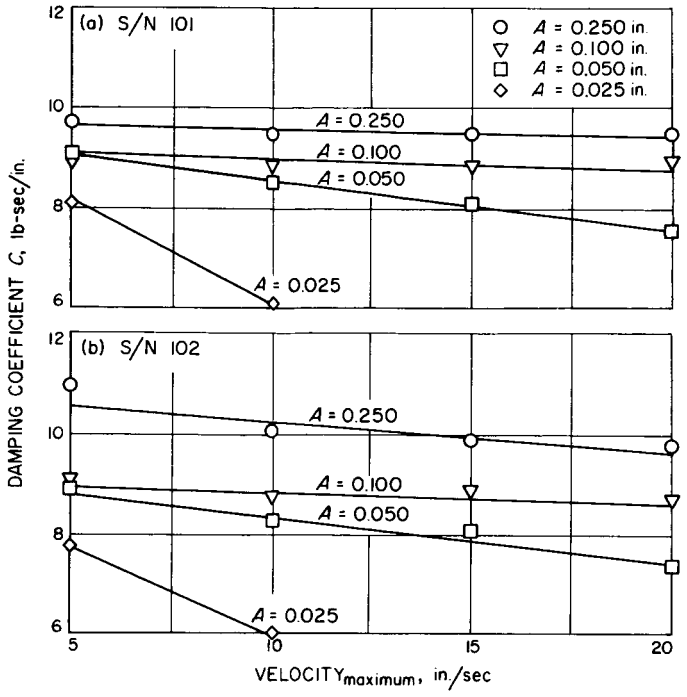

Fig. 25. Bellows damper: C vs velocity

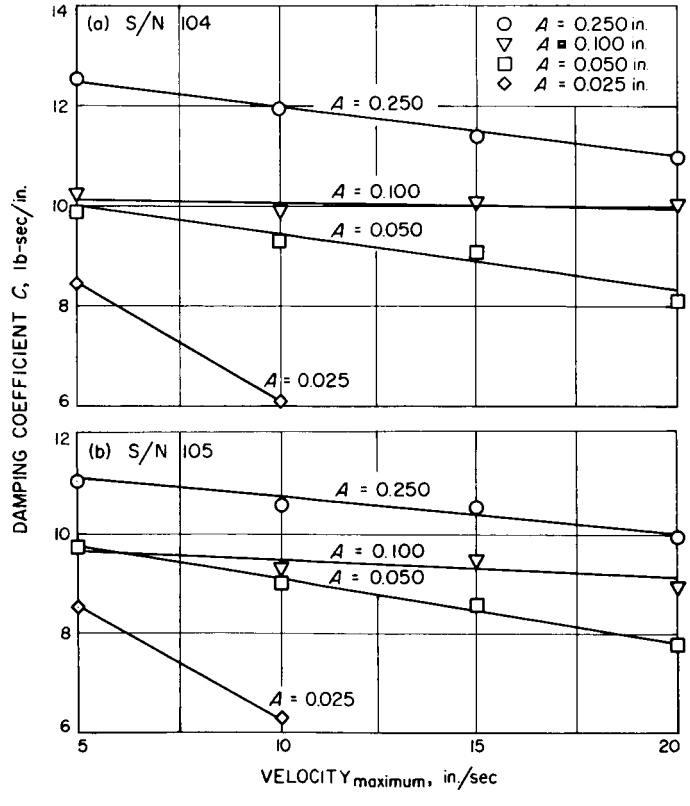

Fig. 26. Bellows damper: C vs velocity

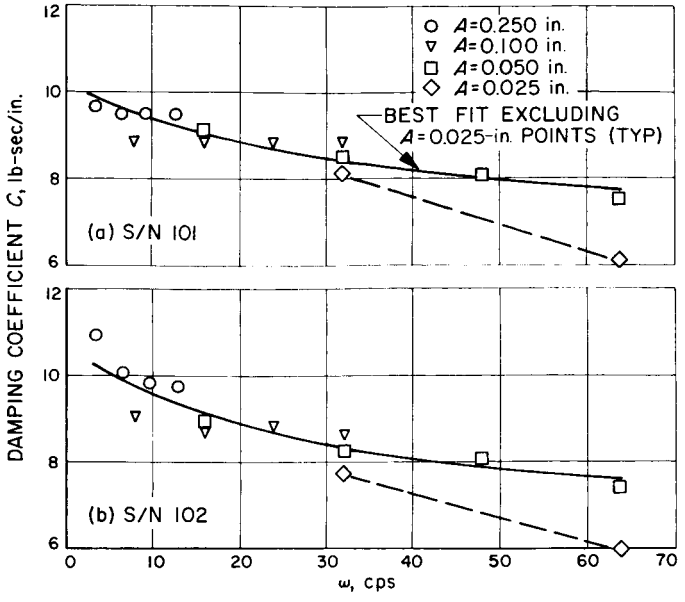

Fig. 27. Bellows damper: C vs frequency

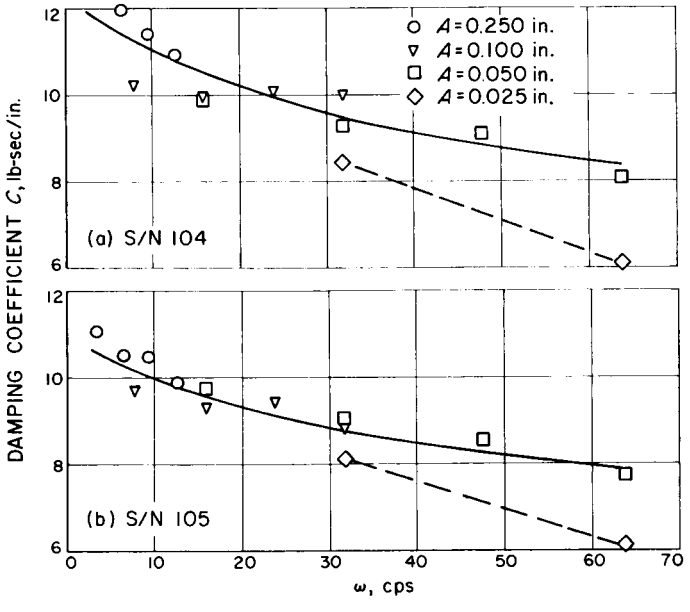

Fig. 28. Bellows damper: C vs frequency

poorer "linear" behavior. Qualitatively, these differences were caused by:

1. The damping fluid-containing "cylinder" consisting of numerous varying section flow channels formed by the bellows convolutions. The viscous loss through these channels was not accounted for in the design calculations.

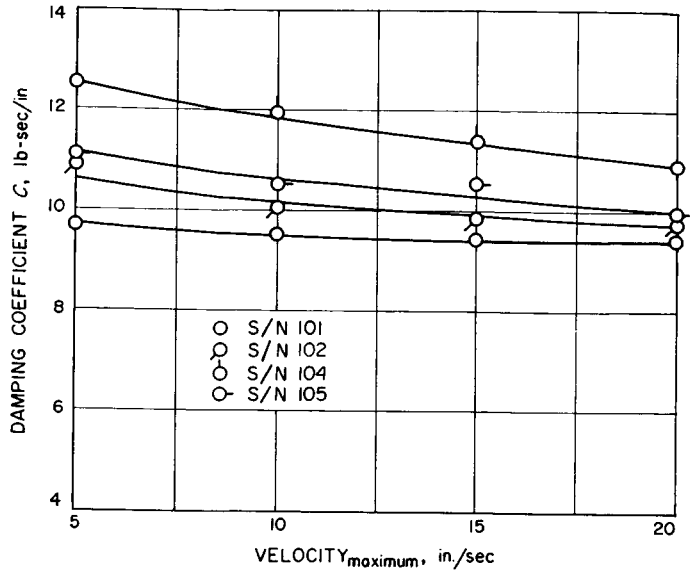

Fig. 29. Bellows damper: effect of manufacturing tolerances

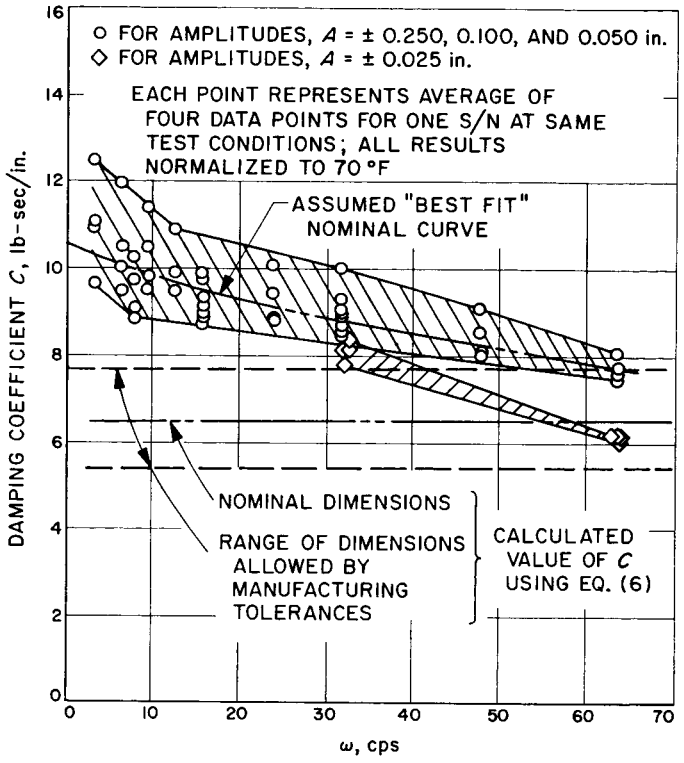

Fig. 30. Bellows damper: test-data summary

2. For tests run at a fixed amplitude, the internal pressure on the fluid-supply side of the damper increases proportionally with $\dot{x}_{max}$ which dilates these flow channels, thus decreasing this local contribution to the damping coefficient, as shown in Figs. 25 and 26.

3. This lack of rigidity of the containing "cylinder" causes a volume increase on the high-pressure end of the damper and results in less flow through the restriction orifice and a reduction in damping coefficient. For tests run at the same $\dot{x}_{max}$ at different amplitudes, this relative reduction in flow increases with lower values of amplitude, as can be seen in Figs. 25 and 26.

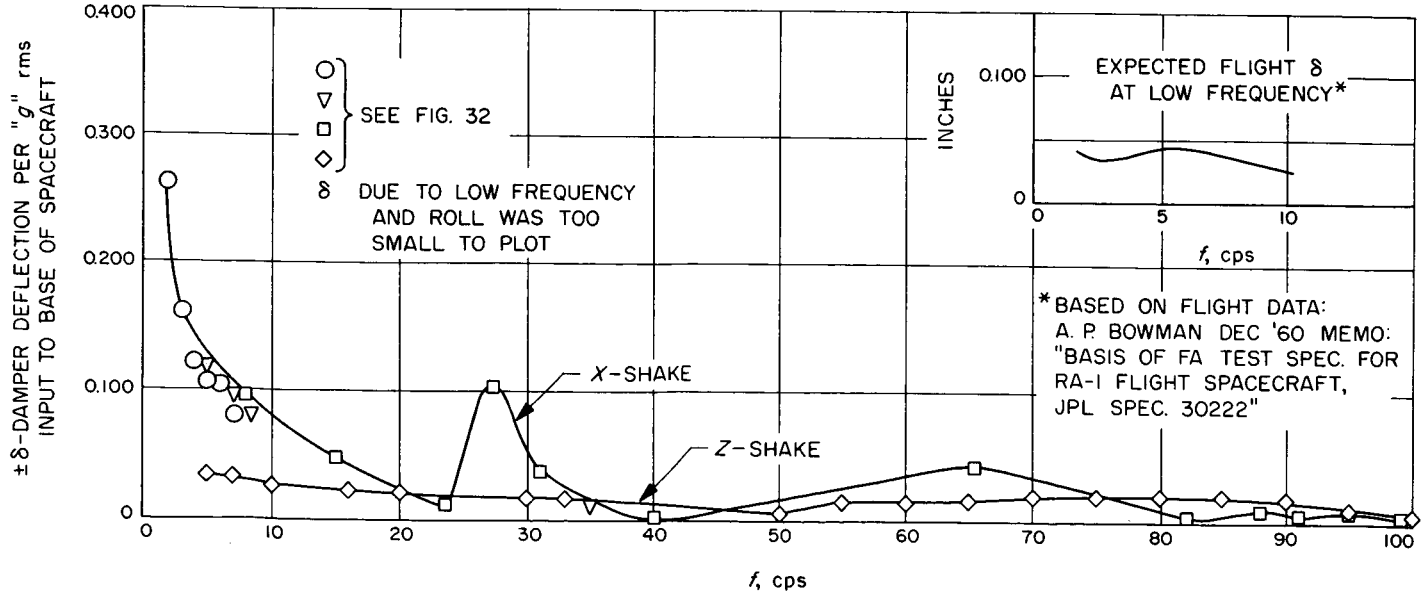

Fig. 31. STM test: damper deflection A vs frequency

The test results, however, show that for a particular design configuration, the Bellows dampers demonstrate good performance consistency between units. A large amount of the data scatter may be explained by the very poor means of measuring fluid temperatures. This data scatter would undoubtedly be considerably reduced if a better means of temperature measurement were incorporated into the design.

Life tests were conducted on both types of dampers over the range of frequencies, amplitudes, and temperatures expected in flight in order to determine the life-performance margin over the estimated 10,000 cycles for flight units. The four *Ranger* test units went through the target 120,000 cycles with no change in performance and a maximum leakage of 0.5 gm of the damping fluid. Tests were continued to over 600,000 cycles on two of the units, resulting in excessive leakage but less than 10% reduction in damping coefficient. For reference, part of the acceptance testing for the flight units requires a loss of less than 0.05 gm after cycling to the estimated flight cycles. All four Bellows damper units were driven in excess of 750,000 cycles, revealing no failure, no leakage, and no change in performance.

The final confirmation of the adequacy of the damper to substantially damp the lower vibration modes of the solar panels and position them within the available space envelope was determined during the Structural-Test-Model tests. This model, which structurally and dynamically duplicates the complete spacecraft in its flight configuration, is subjected 150% of the conservatively predicted launch vibration environment. As shown in Figs. 31 and 32 the final damper performance is well within the design goals. Only the low frequency, *X*-direction (normal to plane of solar panels), sine-sweep data is given, since all other shake directions and frequency ranges proved to be even less critical. Figures 32 and 33 confirm that the range of test parameters used to test the individual damper units conforms with the actual measured range on the complete spacecraft.

The Structural-Test-Model tests were made using solar-panel dampers having the nominal design damping coefficient $C = 8.0$ lb-sec/in. Since changes in damper temperature and allowable manufacturing tolerances would result in a large change in C (Fig. 3), it was necessary to check the resulting effect on panel damping. Ideally, the effect of these different damping coefficients should be checked by further Structural-Test-Model tests on the complete spacecraft. For a number of reasons (e.g., cost and limited time), this was not feasible; thus, parametric tests were made shaking a single panel on a rigid fixture, as shown in Fig. 34. This fixture was driven at a level intended to duplicate the spacecraft-structure input to the solar panels during the Structural-Test-Model tests (see Tables 1 and 2).

Applying the results of these parametric tests to the maximum solar-panel tip gain (i.e., ratio of panel tip

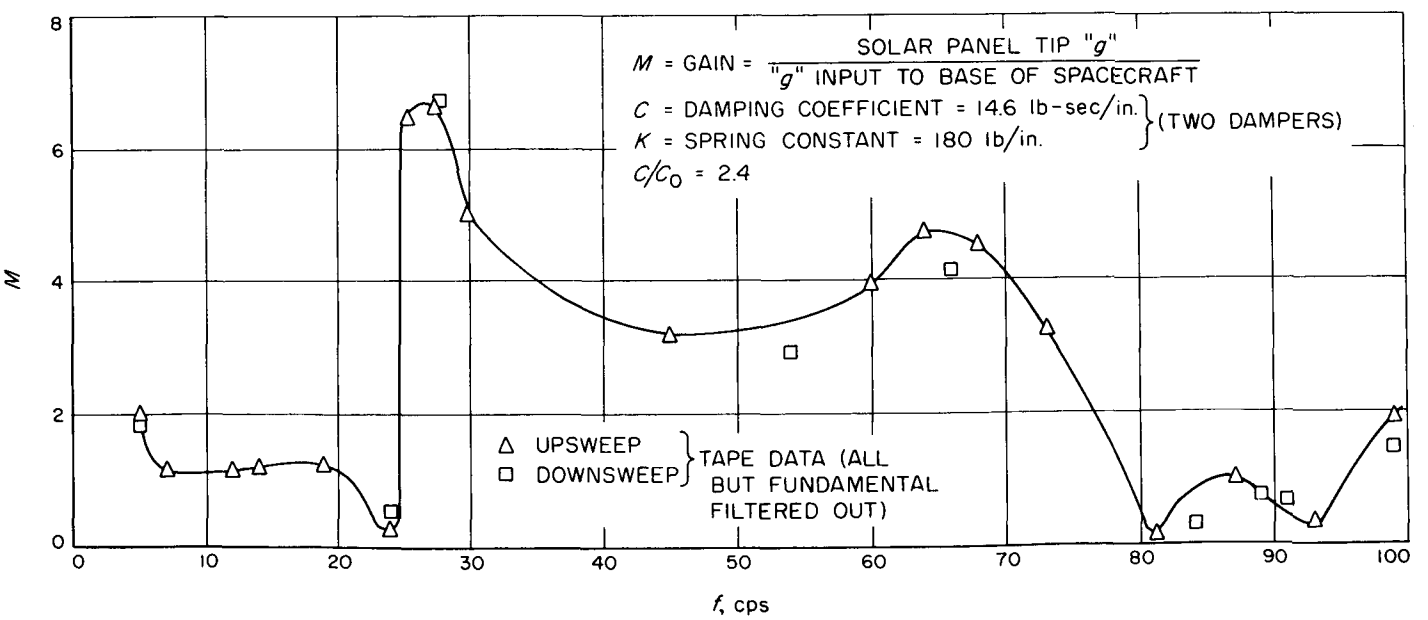

Fig. 32. STM test: solar panel tip gain M vs frequency

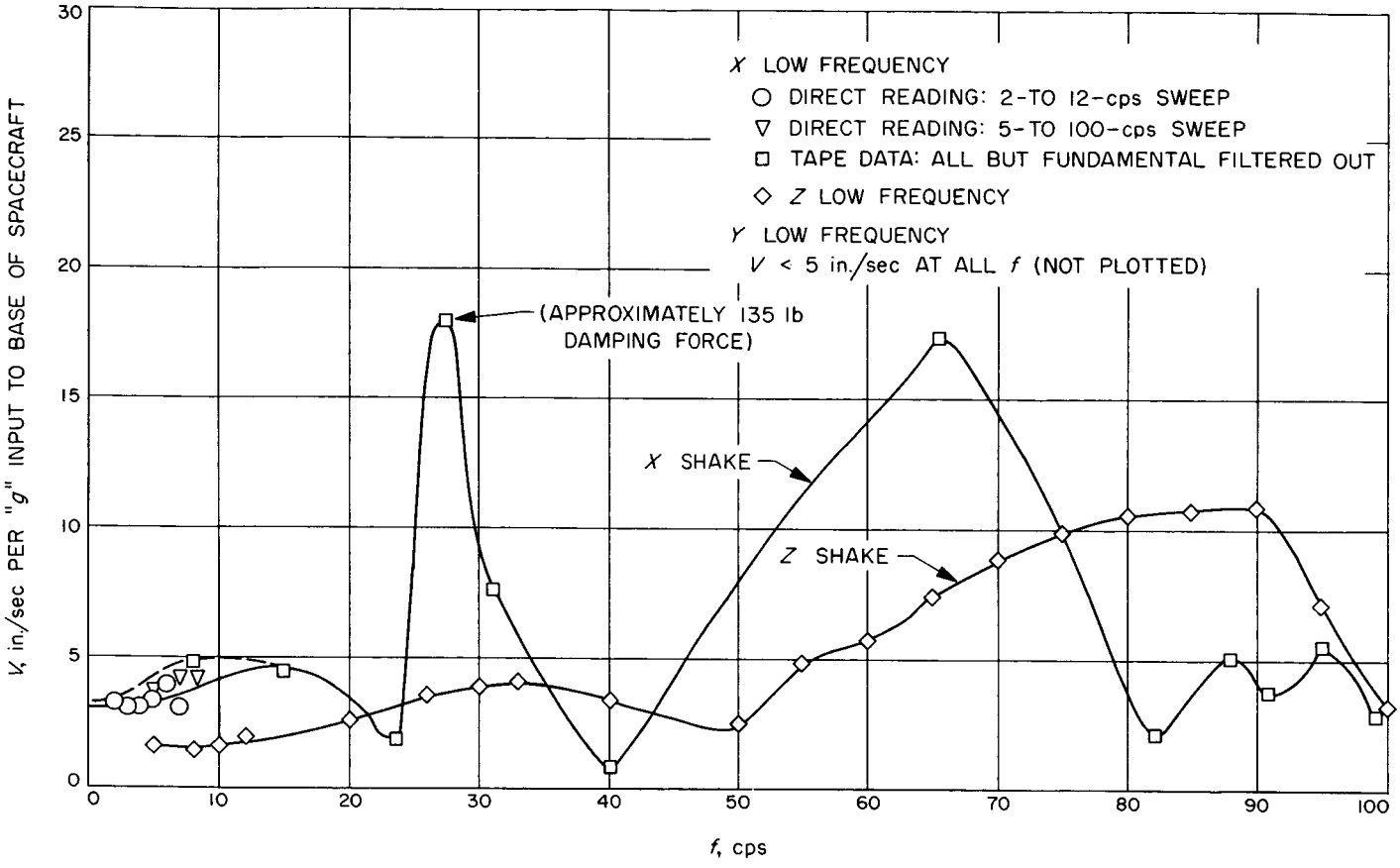

Fig. 33. STM test: damper velocity x_{max} vs frequency

Table 1. Parametric test range[a]

Run	Damping coefficient C = lb-sec/in.		Simulated flight condition
	Side A	Side B	
1	8.0	8.0	Nominal C (at 80°F)
2	4.5	4.5	Minimum C (at 130°F)
3	11.5	11.5	Maximum C (at 50°F)
4	10.3	6.3	Maximum variation of C for two dampers (at 80°F)
5	8.0	Solid link	Malfunction of one damper by "freezing up"

[a]Cf. Fig. 3.

Table 2. Parametric test results

Conditions of run	Solar-panel tip gain expected on complete spacecraft
1	6.8
2	5.6
3	8.5
4	6.9
5	11.9

acceleration to the input acceleration to the spacecraft base) gives the results shown in Table 2.

The Bellows Damper D124911 damping-coefficient test-data reduction[3] follows:

Assumptions:

$$F = C\dot{x} + kx$$

$$x = A \sin \omega t$$

$$\dot{x} = A\omega \cos \omega t$$

$$k = f(C\,|\dot{x}|) = a_0 + a_1(C\,|\dot{x}|) + a_2(C\,|\dot{x}|)^2$$

$$F_{measured} = F_{max}$$

Then

$$F = CA\omega \cos \omega t + [a_0 + a_1 CA\omega\,|\cos \omega t| + a_2 C^2 \omega^2 \cos^2 \omega t]\, A \sin \omega t$$

[3]See footnote 2.

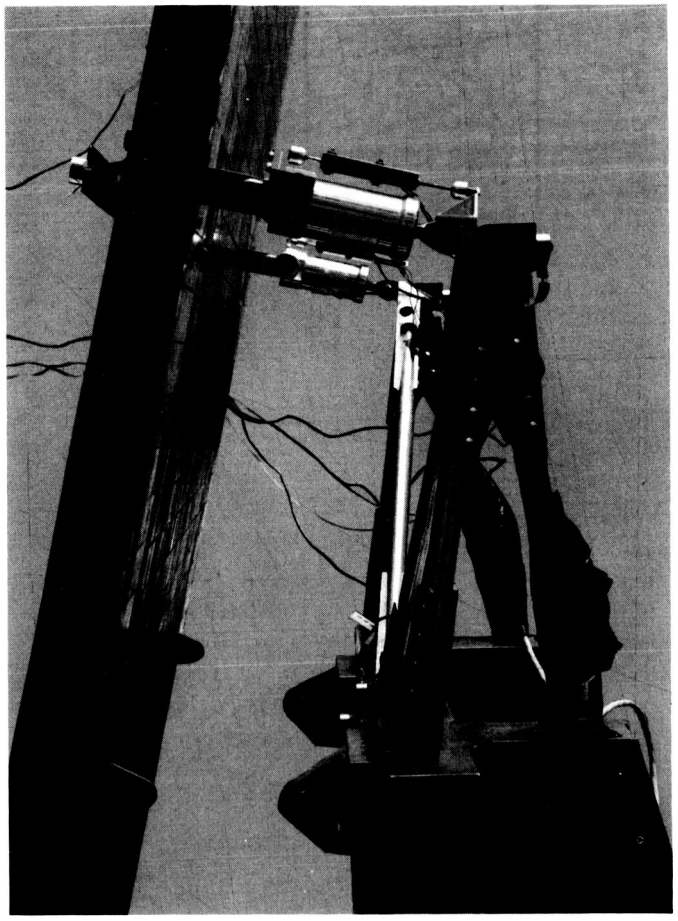

Fig. 34. Damping-coefficient parametric-test setup

Definition:

τ is that value of t which maximizes F. Consequently, τ satisfies the equation:

$$\left.\frac{dF}{dt}\right|_{\tau} = -CA\omega^2 \sin\omega\tau + a_0 A\cos\omega\tau + a_1 CA^2\omega^2(\cos^2\omega\tau - \sin^2\omega\tau)\,\text{sign}(\cos\omega\tau) + a_2 C^2A^3\omega^3\cos\omega\tau(1 - 2\sin^2\omega\tau) = 0$$

One way to solve for τ is to iterate using Newton's method. In Newton's method, if

τ_n = the n^{th} iterate on τ

τ_{n+1} = the $n + 1^{\text{st}}$ iterate on τ

d_0 = the function for which the desired root is τ

d_1 = the time derivative of d

then

$$\tau_{n+1} = \tau_n - \frac{d_0(\tau_n)}{d_1(\tau_n)}$$

$$d_0(\tau) \equiv \frac{1}{A\omega}\left.\frac{dF}{dt}\right|_{\tau} = -C\omega\sin\omega\tau + (a_0 + a_2C^2A^2\omega^2)\cos\omega\tau + 2a_2C^2A^2\omega^2\cos^3\omega\tau + a_1CA\omega(2\cos^2\omega\tau - 1)\,\text{sign}(\cos\omega\tau)$$

$$d_1(\tau) \equiv \frac{d}{dt}[d_0(t)]\Big|_{\tau} = -C\omega^2\cos\omega\tau - (a_0 + a_2C^2A^2\omega^2)\,\omega\sin\omega\tau - 6a_2C^2A^2\omega^2\cos^2\omega\tau\sin\omega\tau - 4a_1CA\omega^2\sin\omega\tau\,|\cos\omega\tau|$$

Once τ is found,

$$F_{measured} = CA\omega\cos\omega\tau + [a_0 + a_1CA\omega\,|\cos\omega\tau| + a_2C^2A^2\omega^2\cos^2\omega\tau]\,A\sin\omega\tau$$

or

$$C^2[a_2A^3\omega^2\sin\omega\tau\cos^2\omega\tau] + C[A\omega\cos\omega\tau(1 + a_1A\sin\omega\tau)\,\text{sign}(\cos\omega\tau)] - [F_{measured} - a_0A\sin\omega\tau] = 0$$

Let

$h_1 = 2a_2A^3\omega^2\sin\omega\tau\cos^2\omega\tau$ $\qquad g_1 = h_3/h_2$

$h_2 = A\omega\cos\omega\tau\,[1 + a_1A\sin\omega\tau\,\text{sign}(\cos\omega\tau)]$ $\qquad g_2 = h_1/h_2$

$h_3 = F_{measured} - a_0A\sin\omega\tau$

Then, if $5/8\,(g_1g_2)^3 \leq 10^{-5}$

$$C = g_1 - \frac{1}{2}g_1^2g_2 + \frac{1}{2}g^3g_2^2 - \frac{5}{8}g_1^4g_2^3$$

and if $5/8\,(g_1g_2)^3 > 10^{-5}$

$$C = -\frac{h_2}{h_1} + \left[\left(\frac{h_2}{h_1}\right)^2 + \frac{2h_3}{h_1}\right]^{1/2}$$

The plus sign in front of the bracket is the result of considering the limits of the two values (from the quadratic formula) for C as a_2 approaches zero (or from the observation that C must be ≥ 0).

Since τ depends on C, and C depends on τ, an iterative procedure is used to solve for both. It is expected that $a_1 C\dot{x}$ and $a_2 C^2\dot{x}^2$ will be small relative to a_0, so the initial values used for the C and τ iteration are based on the values for a_1 and a_2 equal to zero.

$$C_{(0)} = \frac{F_{measured} - a_0 A/4}{A\omega(1 + a_1 A/4)}; \qquad \tau_{(0)} = \frac{1}{\omega}\tan^{-1}\frac{a_0}{C_{(0)}\omega}$$

It is further desirable to normalize the values of C to a common temperature (70°F, in this case).

$$C_{norm} = \frac{\mu_{70°F}}{\mu} \equiv C\,(\text{RATI}\phi)$$

RATIϕ is approximated by

$$\text{RATI}\phi = \begin{cases} 1.000 + 0.100x & -4 \leq x \leq 0 \\ 1.000 + 0.100x + 0.005156x^2 & 0 < x < 7.5 \\ 2.04 + 0.202\,(x - 7.5) & 7.5 \leq x \leq 13 \end{cases}$$

where

$$x = \frac{1}{10}[(\text{Temperature}) - 70°\text{F}]$$

To normalize ϕ

$$\phi_{norm} = \tan^{-1}\frac{Ak\,(C_{norm}\dot{x})}{C_{norm}A\omega}$$

VI. DISCUSSION

The results of this damper development show that employment of point dampers, in series with the links that attach large multi-moded components to a spacecraft structure, is effective in reducing the vibration environment to which the component is subjected during launch. Although the object of this development was to provide a better environment for the solar panels, there is some evidence that indicates a bonus effect of the dampers absorbing some of the energy of critical modes of other portions of the spacecraft.

The particular damper design for the *Ranger* flight was selected on the basis that it would do the job reliably and could be available within the scheduled time. The feature of linearity of damping force with velocity, which this damper demonstrates, is desirable from a structural analysis point of view; however, it has not been shown that this is either necessary or optimum. It is believed that the alternate Bellows damper would probably demonstrate an equally satisfactory performance and without the potential leakage problem inherent in the *Ranger* dampers. Possibly a nonfluid damper based on the hysteretic/visco-elastic principle of absorbing energy could be developed to do the same attenuation job. More work is necessary in this area.